INORGANIC CHEMISTRY
FRONTIERS

RESEARCH ARTICLE

View Article Online
View Journal | View Issue

Cite this: *Inorg. Chem. Front.*, 2023, **10**, 824

Optimizing the pore space of a robust nickel–organic framework for efficient C_2H_2/C_2H_4 separation†

Xiuping Liu,‡[a] Yue Li,‡[b] Chunlian Hao, [b] Weidong Fan, *[b] Wei Liu,[a] Jingquan Liu [a] and Yijun Wang*[a]

The separation of acetylene (C_2H_2) from ethylene (C_2H_4) is an important but challenging process in industry because of their similar physical properties and kinetic molecular sizes. Here, we presented a robust nickel–organic framework (UPC-22) with intrinsic hydrogen bonds and one-dimensional functionalized channels, offering efficient purification of C_2H_4. UPC-22 exhibits excellent chemical stability at various pH values from 1 to 11 and a high C_2H_2/C_2H_4 selectivity of 4.8 at 273 K. Actual breakthrough experiments further demonstrate that UPC-22 is a promising potential adsorbent for C_2H_2/C_2H_4 separation with a C_2H_4 productivity of 1.07 mmol g^{-1}. Grand canonical Monte Carlo simulation and density functional theory indicate that the unsaturated Ni^{II} sites and uncoordinated carboxylate groups with an additional contribution from π···π packing between aromatic rings provide stronger multipoint interactions with C_2H_2 over C_2H_4. This study offers practical guidance to fabricate durable materials for C_2H_2/C_2H_4 separation in real industrial scenarios.

Received 12th November 2022,
Accepted 12th December 2022

DOI: 10.1039/d2qi02398a

rsc.li/frontiers-inorganic

Introduction

Ethylene (C_2H_4), as one of the most important chemical feedstocks, is widely used to manufacture various chemicals and polymers. More than 170 million tons of C_2H_4 are produced annually through petroleum cracking and ethane dehydrogenation.[1] During the C_2H_4 production, trace amounts of acetylene (C_2H_2, about 1%) are always mixed with the resultant C_2H_4-containing gases, which can cause catalyst poisoning and hinder further utilization of C_2H_4 in the chemical and polymer industries.[2] Therefore, the purification of C_2H_4 is considered to be one of the most critical industrial processes.[3] However, the similar physical properties and molecular sizes of C_2H_2 and C_2H_4 also make their separation quite challenging. Currently, industrial technologies for C_2H_2/C_2H_4 separation, including partial hydrogenation and solvent extraction, are very costly and energy-intensive.[4–6] In contrast, adsorptive separation based on porous materials has attracted extensive attention in academia and industry because of its high efficiency and low-energy consumption.[7–11]

Metal–organic frameworks (MOFs) exhibit excellent application prospects in adsorption and separation because of their designable structures and tunable pore sizes/functionalities.[12–18] Recently, MOFs have attracted increasing attention for their potential applications in C_2 hydrocarbon separation (C_2H_2/C_2H_4, C_2H_4/C_2H_6, and C_2H_2/C_2H_6, *etc.*).[19–25] To improve the separation performance of MOFs, several strategies have been proposed, including pore size customization, pore surface functionalization, open metal sites (OMSs), *etc.* Since the first porous MOF (M′MOF) for C_2H_2/C_2H_4 separation was reported in 2011, researchers have taken considerable effort to implement some porous MOFs to achieve their efficient separation.[26–29] For example, Li *et al.* achieved high C_2H_2/C_2H_4 selectivity through NbU-8 with ultra-microporous building units and –OH groups, which was attributed to the supramolecular interaction between the framework and C_2H_2 molecules.[30] The C–H···O/N hydrogen-bonding interaction between MOFs and gas molecules plays a significant role in the selective adsorption of gas molecules.[31] A special Cu-MOF (NbU-1) synthesized by Zhou *et al.* showed one of the highest kinetic separation efficiencies of C_2H_2/C_2H_4 through the cooperation of Cu···C≡C interactions and Lewis-basic sites forming the H–C≡C–H···N (pyridyl) hydrogen bond.[32] Sun *et al.* reported that ZNU-3 with intrinsic hydrogen bonding

[a]*School of Materials Science and Engineering, Linyi University, Linyi, Shandong 276000, China. E-mail: wangyijun@lyu.edu.cn*
[b]*School of Materials Science and Engineering, China University of Petroleum (East China), Qingdao, Shandong, 266580, China. E-mail: wdfan@upc.edu.cn*
†Electronic supplementary information (ESI) available: Simulation details, SEM images, TG curves, IR spectrum, and gas adsorption results. CCDC 2167452. For ESI and crystallographic data in CIF or other electronic format see DOI: https://doi.org/10.1039/d2qi02398a
‡These authors contributed equally.

exhibited excellent C_2H_2 separation performance in the presence of C_2H_4, C_2H_6, and CO_2 due to the synergistic hydrogen bonding of carboxylate groups and π···π packing interactions.[33] Therefore, an effective method to achieve special recognition for C_2H_2 is to introduction of particular functional sites, such as OMSs, functional groups, and hydrogen-bonding acceptors.

Based on the above considerations, we constructed a novel nickel-MOF UPC-22 ($[Ni_3(\mu_3\text{-}OH)_2(HATTCA)(H_2O)_4]$, H_3ATTCA = 2-amino-[1,1:3,1-terphenyl]-4,4,5-tricarboxylic acid), featuring multiple types of pores and specific pore space forming stronger host–guest interactions. UPC-22 not only has excellent thermal and chemical stability, but also has two types of optimized functional channels with OMSs, $-NH_2$, and uncoordinated carboxylate groups. Breakthrough experiments show that UPC-22 can efficiently separate C_2H_4 from the C_2H_2/C_2H_4 mixture. Grand canonical Monte Carlo (GCMC) simulation and density functional theory (DFT) reveal that the unsaturated Ni^{II} sites and hydrogen bonding from carboxylate groups play a significant role in C_2H_4 purification.

Results and discussion

Crystal structure of UPC-22

Conventional rod-shaped UPC-22 crystallizes in an orthorhombic system with the *I2b2* space group (Fig. S1 and Table S1†). The Ni^{2+} ions in the framework adopt an octahedral geometry with oxygen atoms from carboxylate and H_2O, which are then arranged into 1D metal chains (Fig. 1c). Adjacent chains are connected by ligands into two-dimensional sheets. Only two of the three carboxylate groups of each H_3ATTCA ligand are coordinated to the nickel ions, and the other are protonated and hydrogen-bonded to the adjacent ligand (Fig. 1d). These hydrogen bond arrays connect the layers into a three-dimensional framework with one-dimensional channels. The length of hydrogen bonds (1.901 Å) is largely shorter than the sum of the van der Waals radii of the H and O atoms (2.6 Å), indicating that a strong hydrogen bonding exists (Fig. 1d). There are two rhombic channels in UPC-22 (Fig. 1e): the smaller channel A (Fig. 1a) with approximate dimensions of 2.8 × 16 $Å^2$ and the larger channel B (Fig. 1b) with the dimensions of 6.5 × 15 $Å^2$. Furthermore, there are many open Ni^{2+} sites and carboxylate groups, which can be regarded as active sites around the rhombic channels and provide a stronger binding affinity for C_2H_2 than C_2H_4.

Stability of UPC-22

The stability of the adsorbent plays a significant role in practical application. Therefore, we evaluated the thermal and chemical stability of UPC-22. Thermogravimetric analysis (TGA) confirmed the thermal stability of the as-synthesized UPC-22 (Fig. S2†). When heated to 150 °C, the loss of guest water molecules was observed. Up to 375 °C, a substantial decline in quality was observed, and the structure began to col-

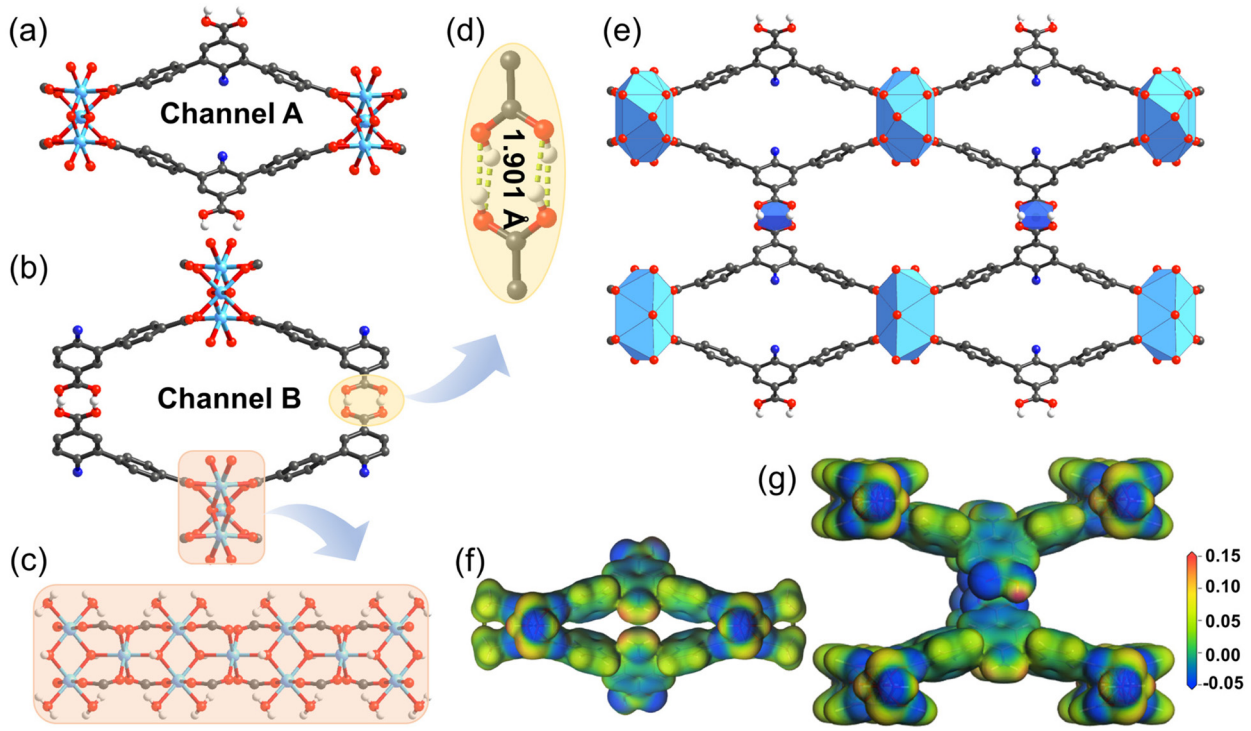

Fig. 1 Crystal structure of UPC-22. (a) and (b) The different channels of the framework in UPC-22; (c) the infinite secondary building units (iSBUs) comprised of one-dimensional (1D) nickel(II) chains; (d) view of the connection of the ligand by hydrogen bonds; (e) the three-dimensional framework with one-dimensional channels along the *b*-axis; (f) and (g) electrostatic potential (ESP) onto the pore surface of Ni-MOF mapped onto the 0.05 e $Å^{-3}$ electron density isosurfaces. Ni, O, N and C are represented by green, red, blue, and gray, respectively.

lapse, which was consistent with the result of variable temperature powder X-ray diffraction (PXRD; Fig. S3†). The PXRD of bulk crystalline samples was conducted to examine the purity and chemical stability (Fig. 2). The chemical stability was determined by soaking UPC-22 samples in solutions of different pH values. There are no obvious peak changes in the PXRD patterns; thus, UPC-22 can retain its structural integrity over 24 h in water in different acidic/basic aqueous solutions (pH, 1–11). The high stability of UPC-22 can be attributed to the stable multicore nickel metal chain and the strong Ni–O bond with a length of 2.034–2.093 Å. In a word, thermal and chemical stability in acidic, basic, and neutral aqueous solutions makes UPC-22 an extraordinary adsorbent.

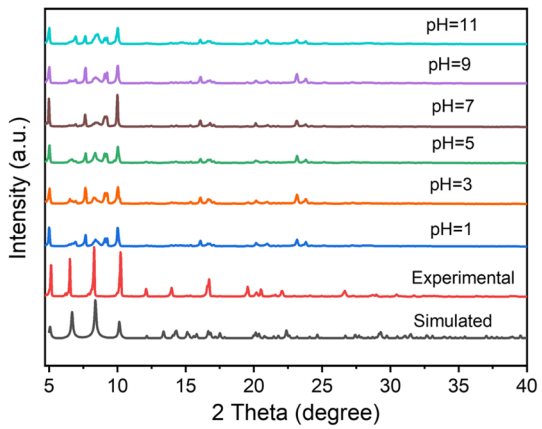

Fig. 2 PXRD patterns of UPC-22 simulated from X-ray crystal diffraction data, experimental and samples sustained in a solution of a given pH, respectively.

Permanent porosity

The permanent porosity of activated UPC-22 was measured using the N_2 sorption isotherm at 77 K. As shown in Fig. 3a, UPC-22 with a typical reversible type-I N_2 adsorption isotherm shows a saturated uptake of 165.6 $cm^3\ g^{-1}$, revealing the permanent porosity of the microporous material. The corresponding Brunauer–Emmett–Teller (BET) surface area and total pore volume are 486.3 $m^2\ g^{-1}$ and 0.26 $cm^3\ g^{-1}$, respectively. In addition, there are two pore systems of around 3.8 Å and 6.5 Å (Fig. 3a), which is consistent with the single crystal data.

Adsorption and separation of C_2 hydrocarbons

Considering the two types of rhombic channels decorated with carboxylate O atoms as hydrogen bond acceptors and dense open Ni^{II} sites, we further investigated the adsorption performance of UPC-22 for C_2H_2, C_2H_4, and C_2H_6. As shown in Fig. 3b and Fig. S5,† the single adsorption isotherms of C_2H_2, C_2H_4,

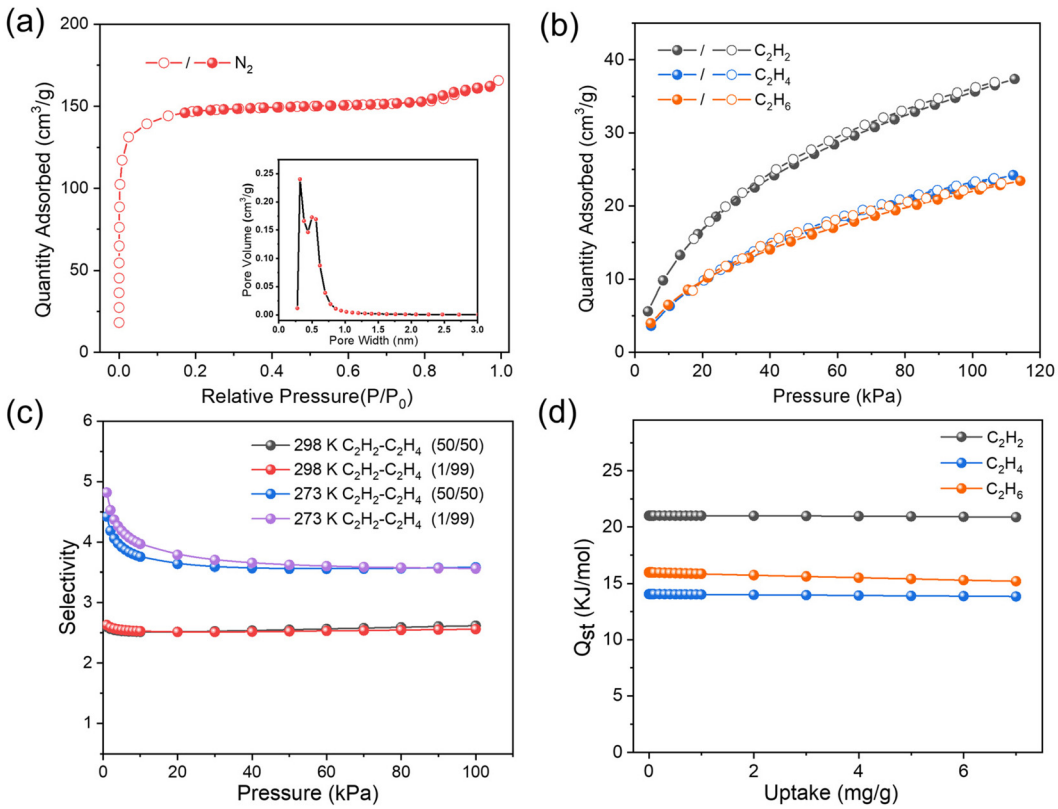

Fig. 3 (a) The N_2 adsorption isotherm in UPC-22 at 77 K and the pore size distribution for UPC-22. (b) The C_2H_2, C_2H_4, and C_2H_6 adsorption isotherms in UPC-22 at 298 K. (c) Adsorption selectivities of UPC-22 calculated by the IAST method for the mixtures of C_2H_2/C_2H_4 at 273 K and 298 K. (d) Isosteric heats of adsorption of C_2H_2, C_2H_4, and C_2H_6.

and C_2H_6 at 298 and 273 K were obtained, respectively. The results show that there are significant differences in the adsorption capacity of UPC-22 for C_2 hydrocarbons. Compared with C_2H_4 and C_2H_6, the type I curve of C_2H_2 has a steeper upward trend, indicating a stronger host–guest interaction between C_2H_2 and the framework. The C_2H_2 uptake of UPC-22 under 1 bar is 46.8 $cm^3\ g^{-1}$ at 273 K and 37.4 $cm^3\ g^{-1}$ at 298 K. For C_2H_4 and C_2H_6, the maximum adsorption capacities are relatively small, only 29.2 and 28.6 $cm^3\ g^{-1}$ at 273 K and 24.2 and 23.4 $cm^3\ g^{-1}$ at 298 K, respectively. The large adsorption capacity of C_2H_2 with the uptake ratio of C_2H_2/C_2H_4 is 1.55 at 298 K, which is greater than the reported values for the MOF-74 series (1.21–1.36),[34] ZJNU-115 (1.26),[31] ZJNU-119 (1.33),[35] and ZJNU-7 (1.4).[15] The great differences in the adsorption capacity between C_2H_2, C_2H_4, and C_2H_6 in UPC-22 revealed the large potential for one-step purification of C_2H_4 and C_2H_6. Then, the adsorption enthalpies (Q_{st}) of the three gases were calculated based on the Clausius-Clapeyron equation (Fig. 3d and Fig. S6†). The Q_{st} values for C_2H_2, C_2H_4, and C_2H_6 at zero loading are 21.1, 15.9, and 14.1 kJ mol^{-1}, respectively. The Q_{st} of UPC-22 for C_2H_2 is much higher than that for C_2H_4 over the entire loading range, indicating that UPC-22 has a strong affinity for C_2H_2. For practical application, the moderate Q_{st} values of UPC-22 show that it can reduce the energy consumption of adsorbate recovery and adsorbent regeneration.

Inspired by the difference in the adsorption capacity and Q_{st} for C_2H_2, C_2H_4, and C_2H_6, the ideal adsorption solution theory (IAST) calculations were used to evaluate the separation performance of C_2H_2/C_2H_4 and C_2H_2/C_2H_6 in UPC-22. As shown in Fig. 3c and Fig. S7,† the C_2H_2/C_2H_4 adsorption selectivity decreased first and then remained constant, while the C_2H_2/C_2H_6 selectivity showed an increasing trend. At the initial pressure, the corresponding IAST selectivity for C_2H_2/C_2H_4 (v/v, 1 : 99) was 2.7 at 298 K and 4.8 at 273 K; the C_2H_2/C_2H_4 selectivity for the molar ratio of 50 : 50 (v/v) at 298 K and 273 K was 2.6 and 4.4, respectively (Fig. 3c). Obviously, under the ambient conditions, the C_2H_2/C_2H_4 selectivity of UPC-22 is higher than that of most reported promising MOFs, such as MgMOF-74 (2.18),[36] FeMOF-74 (2.08),[37] BSF-1 (2.3),[38] NUM-9a (1.63),[4] NOTT-300 (2.17),[39] and NUM-12a (1.4),[40] but lower than that of some leading MOFs, such as SNNU-40 (4.5)[41] and ZJU-198 (7.2).[42] Furthermore, the C_2H_2/C_2H_6 selectivity is 2.6 and 2.4 at 298 K, corresponding to the ratio of 50 : 50 (v/v) and 1 : 99 (v/v), respectively (Fig. S7†). The above results indicate that UPC-22 is a potential C_2H_2-selective material to purify C_2H_4 and C_2H_6.

Encouraged by the above results, we further tested the actual separation performance of C_2H_2/C_2H_4 and C_2H_2/C_2H_6 under ambient conditions. The experimental breakthrough studies of C_2H_2/C_2H_4 (50 : 50, v/v) and C_2H_2/C_2H_6 (50 : 50, v/v) mixtures were performed using the fully degassed UPC-22 samples under a total flow of 3 mL min^{-1}. The breakthrough curves of the C_2H_2/C_2H_4 and C_2H_2/C_2H_6 mixtures are shown in Fig. 4. For C_2H_2/C_2H_4 mixtures, owing to the low C_2H_4 affinity of UPC-22, the breakthrough of C_2H_4 occurred in the early stage, while C_2H_2 was detected after about 8 min g^{-1} and the productivity was 1.07 mmol g^{-1} (Fig. 4a). UPC-22 can purify the C_2H_2/C_2H_4 mixture into high-purity C_2H_4 (99.99%) at 298 K with good cycling stability (Fig. S11†). The productivity of C_2H_4 in the C_2H_2/C_2H_4 mixture is higher than those of some promising MOFs, such as ZJU-HOF-1 (0.98 mmol g^{-1})[43] and ZnBAIm (0.3 mmol g^{-1}).[44] In addition, the breakthrough study was conducted with C_2H_2/C_2H_6 under the same conditions (Fig. 4b). The penetration of C_2H_6 was first detected, and the penetration time of C_2H_2 was about 7 min g^{-1}.

GCMC and DFT calculations were further carried out to obtain preferential adsorption sites and gain some meaningful insights. First, the adsorption properties of UPC-22 for C_2H_2 and C_2H_4 at 298 K were investigated by GCMC simulations. There are three primary adsorption sites between C_2H_2 and C_2H_4 molecules and the channel surface (Fig. 5a, d and S9–S10†). The adsorbed gas molecules are preferentially located around the open Ni^{II} sites and uncoordinated carboxylate

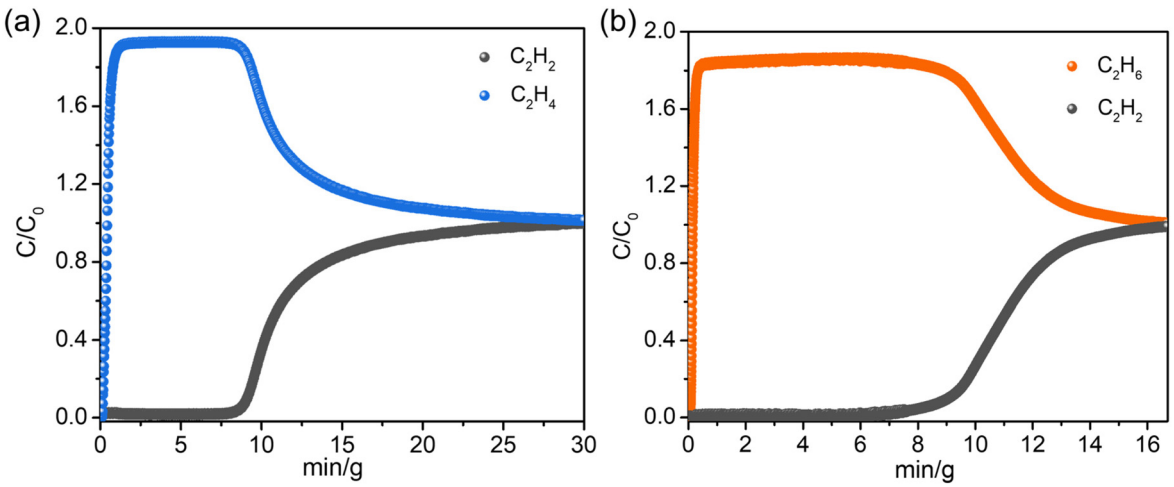

Fig. 4 Column breakthrough curves of UPC-22 for (a) C_2H_2/C_2H_4 and (b) C_2H_2/C_2H_6 mixtures at 298 K and 1 bar.

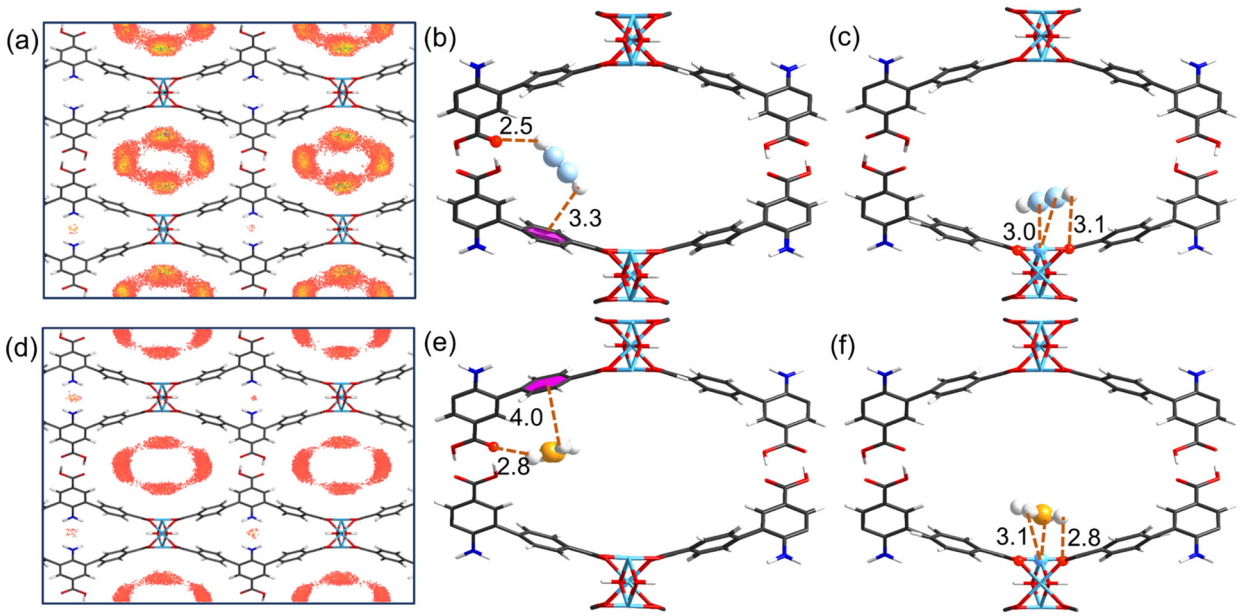

Fig. 5 Results of the GCMC simulations showing preferential binding sites between the adsorbed molecule and UPC-22: (a) C_2H_2 and (d) C_2H_4 at 298 K and 30 KPa; binding sites of C_2H_2 and C_2H_4 in UPC-22 determined by DFT simulations (b–c) and (e–f).

groups in the larger channel B, whereas few near the amine groups of ligands in the channel A with a smaller size. DFT calculations were further conducted to obtain the optimized adsorption geometrical structures and the adsorption energy between C_2H_2/C_2H_4 and the framework. The DFT calculated adsorption sites are in good agreement with the results of GCMC simulations (Fig. 5b, c, 5e, f and Fig. S11†). The adsorption energy of C_2H_2 molecules on open Ni^{II} sites is larger than that of C_2H_4, with the corresponding values of 49.94 and 48.41 kJ mol^{-1} (Fig. 5b and c), which are attributed to the synergistic effect of C–H···O hydrogen bonds and stronger Coulomb attraction between open Ni^{II} sites and C≡C with π electrons. Another adsorption site of C_2H_2 is the non-coordinating carboxylate group and benzene ring with an adsorption energy of 47.78 kJ mol^{-1}, forming strong and multiple O_{-COO}···H–C≡C–H···π hydrogen bonds and van der Waals interactions with close distances of 2.5/3.3 Å (Fig. 5b). In contrast to C_2H_2, the adsorption energy of C_2H_4 at this site (42.50 kJ mol^{-1}) is significantly lower with larger distances between C_2H_4 and the framework (Fig. 5e). Moreover, the results of the electrostatic potential revealed that surface O atoms of non-coordinating carboxylate sites exhibited a strong negative potential, which could attractively interact with H atoms from C_2H_2 and C_2H_4 by forming strong C–H···O hydrogen bonds (Fig. 1f, g and S12†). Furthermore, the adsorption energies of C_2H_2 and C_2H_4 at the $-NH_2$ site in channel A are 47.91 and 37.12 kJ mol^{-1} (Fig. S11†), respectively, indicating that $-NH_2$ is a strong adsorption site, whereas only a few gas molecules are adsorbed (Fig. S9†) due to the small size of channel A (2.8 × 16 $Å^2$) hindering the entry of gas molecules. Thus, the synergy between OMSs/carboxylate sites and appropriate rhombic channels with aromatic π-electrons can create a multi-binding environment to selectively capture C_2H_2 from C_2H_4 and C_2H_6.

Conclusions

In conclusion, a novel robust MOF (UPC-22) containing two types of rhombic channels decorated with uncoordinated –COOH groups, $-NH_2$ groups, and OMSs was successfully constructed by the hydrothermal method. UPC-22 exhibits a high selectivity toward C_2H_2/C_2H_4 (2.7) under ambient conditions, outperforming most of the promising MOFs. Theoretical calculations reveal that the excellent separation performances are mainly attributed to the aromatic channels with abundant functional groups and OMSs that enable stronger interaction with C_2H_2 molecules than that with C_2H_4. The high framework stability and dynamic breakthrough experiments demonstrate its application prospects in ethylene purification in the petrochemical industry.

Experimental and computational section

Materials and measurements

All materials were used in the commercially available form without further purification. The ligand 2-amino-[1,1:3,1-terphenyl]-4,4,5-tricarboxylic acid (H_3ATTCA) was prepared according to previously published procedures.[45] The powder X-ray diffraction (XRD) data were obtained on an X-Pert PRO MPD diffractometer with Cu-Kα radiation. IR spectra were obtained on a Nexus FT-IR spectrometer using KBr pellets in

the frequency range of 4000–400 cm^{-1}. Elemental analyses (C, H, and N) were performed on an instrument EA 1110 elemental analyzer. Thermo-gravimetric analysis (TGA) experiments were conducted from 40 to 900 °C on a Mettler Toledo TGA instrument with a heating rate of 10 °C min^{-1} under a N_2 atmosphere. Low-pressure (<800 torrs) N_2, C_2H_2, C_2H_4, and C_2H_6 adsorption isotherms were obtained using a Micrometrics ASAP 2020 surface area and pore size analyzer. The Brunauer–Emmett–Teller (BET) surface area was calculated from N_2 adsorption isotherms at 77 K. Pore size distribution data were also obtained from the N_2 adsorption isotherms at 77 K based on a non-local density functional theory (NLDFT) model in the Micromeritics ASAP 2020 software package (assuming a slit pore geometry). The breakthrough experiments were performed on dynamic gas breakthrough equipment. The experiments were conducted using a stainless-steel column. The weight of UPC-22 packed in the columns was 0.6267 g. The mixed gas of C_2H_2/C_2H_4 and C_2H_2/C_2H_6 (50/50, v/v) was then introduced with a flow rate of 3 mL min^{-1}. More details of breakthrough equipment are shown in the ESI.†

Synthesis of UPC-22

H_3ATTCA (7.5 mg, 0.02 mmol) and $Ni(NO_3)_2{\cdot}6H_2O$ (30 mg, 0.10 mmol) in 3 mL of DMF (*N*,*N*-dimethylformamide) : H_2O (v/v = 1 : 1) were ultrasonically dissolved in a Pyrex vial. The Pyrex vial was sealed, heated to 100 °C for 3 days, and then cooled to room temperature. The resulting light-green block crystals were washed multiple times with DMF prior to single-crystal X-ray diffraction analysis. Yield: about 72% based on nickel. Elemental analysis calcd (%) for UPC-22: C, 38.24 N, 2.12 H, 3.64; found: C, 38.31 N, 2.19 H, 3.56.

Computational methods

In this work, the adsorption isotherms of pure C_2H_2 and C_2H_4 in UPC-22 were obtained using the Grand Canonical Monte Carlo (GCMC) method implemented in the Materials Studio code.[46] The site-site L–J potential was described with the L–J (12, 6) model, and the electrostatic interaction was calculated *via* the Coulomb law. The cutoff of 8 Å was employed for the L–J interactions. Density functional theory (DFT) was performed to provide the atomic partial charges and electronic potential of the UPC-22 framework and calculate the optimized structures and energies of the C_2H_2 and C_2H_4 interaction with fragmented clusters.[47] Generalized gradient approximation (GGA) with the Perdew-Burke-Ernzerhof (PBE) functional was used to do all-electron spin-unrestricted DFT calculations. DFT-D calculations were performed using the Grimme parameters for the van der Waals correction of gas adsorption. The details of all the calculations are given in the ESI.†

Conflicts of interest

There are no conflicts to declare.

Acknowledgements

This work was supported by the National Natural Science Foundation of China (NSFC, Grant No. 22108113, 22201305), the Natural Science Foundation of Shandong Province (ZR2020QB032), the Fundamental Research Funds for the Central Universities (22CX06024A), and the Outstanding Youth Science Fund Projects of Shandong Province (2022HWYQ-070).

References

1 L. Li, R.-B. Lin, R. Krishna, H. Li, S. Xiang, H. Wu, J. Li, W. Zhou and B. Chen, Ethane/ethylene separation in a metal-organic framework with iron-peroxo sites, *Science*, 2018, **362**, 443–446.
2 Z. L. Ma, P. X. Liu, Z. Y. Liu, J. J. Wang, L. B. Li and L. Tian, Thermally and chemically stable copper(II) metal-organic framework with high performance for gas adsorption and separation, *Inorg. Chem.*, 2021, **60**, 6550–6558.
3 G.-D. Wang, Y.-Z. Li, W.-J. Shi, L. Hou, Y.-Y. Wang and Z. Zhu, One-step C_2H_4 purification from ternary C_2H_6/C_2H_4/C_2H_2 mixtures by a robust metal-organic framework with customized pore environment, *Angew. Chem., Int. Ed.*, 2022, e202205427.
4 S.-Q. Yang, F.-Z. Sun, P. Liu, L. Li, R. Krishna, Y.-H. Zhang, Q. Li, L. Zhou and T.-L. Hu, Efficient purification of ethylene from C_2 hydrocarbons with an C_2H_6/C_2H_2-selective metal–organic framework, *ACS Appl. Mater. Interfaces*, 2021, **13**, 962–969.
5 Q. Hong, W. Wang, S. Chen, K. Chen, M. Liu, H.-X. Zhang and J. Zhang, Host–guest pore space partition in a boron imidazolate framework for ethylene separation, *Chem. Mater.*, 2022, **34**, 307–313.
6 C. Gu, J. Liu, J. Hu and D. Wu, Highly selective separations of C_2H_2/C_2H_4 and C_2H_2/C_2H_6 in metal–organic frameworks via pore environment design, *Ind. Eng. Chem. Res.*, 2019, **58**, 19946–19957.
7 B.-Y. Zhu, T. Zhang, C.-H. Li, J.-W. Cao, Z.-Q. Zhang, W. Qi, G.-Y. Wang, Z.-H. Rong, Y. Wang and K.-J. Chen, A (3,8)-connected metal–organic framework with bending dicarboxylate linkers for C_2H_2/CO_2 separation, *Inorg. Chem.*, 2022, **61**, 4555–4560.
8 Y.-L. Peng, T. Pham, P. Li, T. Wang, Y. Chen, K.-J. Chen, K. A. Forrest, B. Space, P. Cheng, M. J. Zaworotko and Z. Zhang, Robust ultramicroporous metal–organic frameworks with benchmark affinity for acetylene, *Angew. Chem., Int. Ed.*, 2018, **57**, 10971–10975.
9 K. Su, W. Wang, S. Du, C. Ji and D. Yuan, Efficient ethylene purification by a robust ethane-trapping porous organic cage, *Nat. Commun.*, 2021, **12**, 3703.
10 C. Ji, K. Su, W. Wang, J. Chang, E.-S. M. El-Sayed, L. Zhang and D. Yuan, Tunable cage-based three-dimensional covalent organic frameworks, *CCS Chem.*, 2022, **4**, 3095–3105.

11 L. Li, C. Ji, W. Wang, F. Wu, Y.-X. Tan and D. Yuan, The effect of pore sizes on D_2/H_2 separation conducted by MOF-74 analogues, *Inorg. Chem. Front.*, 2022, **9**, 1674–1680.
12 L.-N. Ma, L. Zhang, W.-F. Zhang, Z.-H. Wang, L. Hou and Y.-Y. Wang, Amide-functionalized In-MOF for effective hydrocarbon separation and CO_2 catalytic fixation, *Inorg. Chem.*, 2022, **61**, 2679–2685.
13 X.-W. Gu, J.-X. Wang, E. Wu, H. Wu, W. Zhou, G. Qian, B. Chen and B. Li, Immobilization of lewis basic sites into a stable ethane-selective MOF enabling one-step separation of ethylene from a ternary mixture, *J. Am. Chem. Soc.*, 2022, **144**, 2614–2623.
14 G.-D. Wang, Y.-Z. Li, W.-F. Zhang, L. Hou, Y.-Y. Wang and Z. Zhu, Acetylene separation by a Ca-MOF containing accessible sites of open metal centers and organic groups, *ACS Appl. Mater. Interfaces*, 2021, **13**, 58862–58870.
15 Z. Jiang, L. Fan, P. Zhou, T. Xu, S. Hu, J. Chen, D.-L. Chen and Y. He, An aromatic-rich cage-based MOF with inorganic chloride ions decorating the pore surface displaying the preferential adsorption of C_2H_2 and C_2H_6 over C_2H_4, *Inorg. Chem. Front.*, 2021, **8**, 1243–1252.
16 S. Zou, Z. Di, H. Li, Y. Liu, Z. Ji, H. Li, C. Chen, M. Wu and M. Hong, Stable fluorinated hybrid microporous material for the efficient separation of C_2–C_3 alkyne/alkene mixtures, *Inorg. Chem.*, 2022, **61**, 7530–7536.
17 Z. Jiang, Y. Zou, T. Xu, L. Fan, P. Zhou and Y. He, An aromatic-rich cage-based MOF with inorganic chloride ions decorating the pore surface displaying the preferential adsorption of C_2H_2 and C_2H_6 over C_2H_4, *Dalton Trans.*, 2020, **49**, 3553–3561.
18 Z. Jiang, L. Fan, P. Zhou, T. Xu, J. Chen, S. Hu, D.-L. Chen and Y. He, A hydrostable cage-based MOF with open metal sites and Lewis basic sites immobilized in the pore surface for efficient separation and purification of natural gas and C_2H_2, *Dalton Trans.*, 2020, **49**, 15672–15681.
19 H. Cheng, Q. Wang, M. Ding, Y. Gao, D. Xue and J. Bai, Modifying a partial corn-sql layer-based (3,3,3,3,4,4)-c topological MOF by substitution of OH(-) with Cl(-) and its highly selective adsorption of C_2 hydrocarbons over CH_4, *Dalton Trans.*, 2021, **50**, 4840–4847.
20 S. R. Acharya, A. Elias, K. Tan, S. Jensen, R.-B. Lin, B. Chen, M. D. Gross and T. Thonhauser, Identifying the gate-opening mechanism in the flexible metal–organic framework UTSA-300, *Inorg. Chem.*, 2022, **61**, 5025–5032.
21 Q.-L. Qian, X.-W. Gu, J. Pei, H.-M. Wen, H. Wu, W. Zhou, B. Li and G. Qian, A novel anion-pillared metal–organic framework for highly efficient separation of acetylene from ethylene and carbon dioxide, *J. Mater. Chem. A*, 2021, **9**, 9248–9255.
22 F.-Z. Sun, S.-Q. Yang, R. Krishna, Y.-H. Zhang, Y.-P. Xia and T.-L. Hu, Microporous metal–organic framework with a completely reversed adsorption relationship for C_2 hydrocarbons at room temperature, *ACS Appl. Mater. Interfaces*, 2020, **12**, 6105–6111.
23 S. Geng, E. Lin, X. Li, W. Liu, T. Wang, Z. Wang, D. Sensharma, S. Darwish, Y. H. Andaloussi, T. Pham, P. Cheng, M. J. Zaworotko, Y. Chen and Z. Zhang, Scalable room-temperature synthesis of highly robust ethane-selective metal–organic frameworks for efficient ethylene purification, *J. Am. Chem. Soc.*, 2021, **143**, 8654–8660.
24 H.-J. Lv, J.-W. Zhang, Y.-C. Jiang, S.-N. Li, M.-C. Hu and Q.-G. Zhai, Micropore regulation in ultrastable $[Sc_3O]$-organic frameworks for acetylene storage and purification, *Inorg. Chem.*, 2022, **61**, 3553–3562.
25 Y.-Z. Li, H.-H. Wang, G.-D. Wang, L. Hou, Y.-Y. Wang and Z. Zhu, A Dy_6-cluster-based fcu-MOF with efficient separation of C_2H_2/C_2H_4 and selective adsorption of benzene, *Inorg. Chem. Front.*, 2021, **8**, 376–382.
26 W. Fan, S. B. Peh, Z. Zhang, H. Yuan, Z. Yang, Y. Wang, K. Chai, D. Sun and D. Zhao, Tetrazole-functionalized zirconium metal-organic cages for efficient C_2H_2/C_2H_4 and C_2H_2/CO_2 separations, *Angew. Chem., Int. Ed.*, 2021, **60**, 17338–17343.
27 X. Zhang, M. Fu, H. Liu, Y. Wang, Y. Zou, L. Wang, C. Li, Y. Lu, L. Zhou and X. Cui, A copper-based metal–organic framework with a suitable pore environment for effective ethylene purification, *Inorg. Chem. Front.*, 2022, **9**, 2104–2108.
28 J. Zhao, Q. Li, X.-C. Zhu, J. Li and D. Wu, Highly robust tetranuclear cobalt-based 3D framework for efficient C_2H_2/CO_2 and C_2H_2/C_2H_4 separations, *Inorg. Chem.*, 2020, **59**, 14424–14431.
29 J. Wang, Y. Zhang, P. Zhang, J. Hu, R.-B. Lin, Q. Deng, Z. Zeng, H. Xing, S. Deng and B. Chen, Optimizing pore space for flexible-robust metal–organic framework to boost trace acetylene removal, *J. Am. Chem. Soc.*, 2020, **142**, 9744–9751.
30 Q. Li, N. Wu, J. Li and D. Wu, A highly connected trinuclear cluster based metal–organic framework for efficient separation of C_2H_2/C_2H_4 and C_2H_2/CO_2, *Inorg. Chem.*, 2020, **59**, 13005–13008.
31 L. Fan, P. Zhou, X. Wang, L. Yue, L. Li and Y. He, Rational construction and performance regulation of an In(III)-tetraisophthalate framework for one-step adsorption-phase purification of C_2H_4 from C_2 Hydrocarbons, *Inorg. Chem.*, 2021, **60**, 10819–10829.
32 J. Li, L. Jiang, S. Chen, A. Kirchon, B. Li, Y. Li and H.-C. Zhou, Rational construction and performance regulation of an In(III)-tetraisophthalate framework for one-step adsorption-phase purification of C_2H_4 from C_2 Hydrocarbons, *J. Am. Chem. Soc.*, 2019, **141**, 3807–3811.
33 W.-Q. Sun, J.-B. Hu, Y.-J. Jiang, N. Xu, L.-Y. Wang, J.-H. Li, Y.-Q. Hu, S. Duttwyler and Y.-B. Zhang, Flexible molecular sieving of C_2H_2 from CO_2 by a new cost-effective metal organic framework with intrinsic hydrogen bonds, *Chem. Eng. J.*, 2022, **439**, 135745.
34 X. Cui, K. Chen, H. Xing, Q. Yang, R. Krishna, Z. Bao, H. Wu, W. Zhou, X. Dong, Y. Han, B. Li, Q. Ren, M. J. Zaworotko and B. Chen, Pore chemistry and size control in hybrid porous materials for acetylene capture from ethylene, *Science*, 2016, **353**, 141–144.

35 P. Zhou, X. Wang, L. Yue, L. Fan and Y. He, A microporous MOF constructed by cross-linking helical chains for efficient purification of natural gas and ethylene, *Inorg. Chem.*, 2021, **60**, 14969–14977.
36 S. Xiang, W. Zhou, Z. Zhang, M. A. Green, Y. Liu and B. Chen, Open metal sites within isostructural metal–organic frameworks for differential recognition of acetylene and extraordinarily high acetylene storage capacity at room temperature, *Angew. Chem., Int. Ed.*, 2010, **49**, 4615–4618.
37 E. D. Bloch, W. L. Queen, R. Krishna, J. M. Zadrozny, C. M. Brown and J. R. Long, Hydrocarbon separations in a metal-organic framework with open iron(II) coordination sites, *Science*, 2012, **335**, 1606–1610.
38 Y. Zhang, L. Yang, L. Wang, S. Duttwyler and H. Xing, A microporous metal-organic framework supramolecularly assembled from a Cu^{II} dodecaborate cluster complex for selective gas separation, *Angew. Chem., Int. Ed.*, 2019, **58**, 8145–8150.
39 S. Yang, A. J. Ramirez-Cuesta, R. Newby, V. Garcia-Sakai, P. Manuel, S. K. Callear, S. I. Campbell, C. C. Tang and M. Schröder, Supramolecular binding and separation of hydrocarbons within a functionalized porous metal–organic framework, *Nat. Chem.*, 2015, **7**, 121–129.
40 Q. Zhang, S.-Q. Yang, L. Zhou, L. Yu, Z.-F. Li, Y.-J. Zhai and T.-L. Hu, Pore-space partition through an embedding metal-carboxylate chain-induced topology upgrade strategy for the separation of acetylene/ethylene, *Inorg. Chem.*, 2021, **60**, 19328–19335.
41 Y. P. Li, Y. N. Zhao, S. N. Li, D. Q. Yuan, Y. C. Jiang, X. Bu, M. C. Hu and Q. G. Zhai, Ultrahigh-uptake capacity-enabled gas separation and fruit preservation by a new single-walled nickel-organic framework, *Adv. Sci.*, 2021, **8**, 2003141.
42 L. Zhang, K. Jiang, M. Jiang, D. Yue, Y. Wan, H. Xing, Y. Yang, Y. Cui, B. Chen and G. Qian, A highly stable amino-coordinated MOF for unprecedented block off N_2 adsorption and extraordinary CO_2/N_2 separation, *Chem. Commun.*, 2016, **52**, 13568–13571.
43 X. Zhang, J.-X. Wang, L. Li, J. Pei, R. Krishna, H. Wu, W. Zhou, G. Qian, B. Chen and B. Li, A rod-packing hydrogen-bonded organic framework with suitable pore confinement for benchmark ethane/ethylene separation, *Angew. Chem., Int. Ed.*, 2021, **60**, 10304–10310.
44 D. Luo, Y.-L. Peng, M. Xie, M. Li, A. A. Bezrukov, T. Zuo, X.-Z. Wang, Y. Wu, Y. Y. Li, A. R. Lowe, M. a. Chorążewski, Y. Grosu, Z. Zhang, M. J. Zaworotko, X.-P. Zhou and D. Li, Improving ethane/ethylene separation performance under humid conditions by spatially modified zeolitic imidazolate frameworks, *ACS Appl. Mater. Interfaces*, 2022, **14**, 11547–11558.
45 W. Fan, H. Lin, X. Yuan, F. Dai, Z. Xiao, L. Zhang, L. Luo and R. Wang, Expanded porous metal–organic frameworks by SCSC: organic building units modifying and enhanced gas-adsorption properties, *Inorg. Chem.*, 2016, **55**, 6420–6425.
46 A. Gupta, S. Chempath, M. J. Sanborn, L. A. Clark and R. Q. Snurr, Object-oriented programming paradigms for molecular modeling, *Mol. Simul.*, 2003, **29**, 29–46.
47 B. Delley, From molecules to solids with the $DMol^3$ approach, *J. Chem. Phys.*, 2000, **113**, 7756–7764.